Beating spatio-temporal coupling: implications for pulse shaping and coherent control experiments

Daan Brinks,[1,*] Richard Hildner,[1,2] Fernando D. Stefani,[1,3] and Niek F. van Hulst[1,4]

[1]*ICFO—Institut de Ciencies Fotoniques, Mediterranean Technology Park, 08860 Castelldefels (Barcelona), Spain*
[2]*Currently with Experimentalphysik IV, Universität Bayreuth, 95440 Bayreuth, Germany*
[3]*Currently with Departamento de Física & Instituto de Física de Buenos Aires (IFIBA, CONICET), Facultad de Ciencias Exactas y Naturales, Universidad de Buenos Aires, 1438 Buenos Aires, Argentina*
[4]*ICREA—Institució Catalana de Recerca i Estudis Avançats, 08015 Barcelona, Spain*
[*]*daan.brinks@icfo.es*

Abstract: Diffraction of finite sized laser beams imposes a limit on the control that can be exerted over ultrafast pulses. This limit manifests as spatio-temporal coupling induced in standard implementations of pulse shaping schemes. We demonstrate the influence this has on coherent control experiments that depend on finite excitation, sample, and detection volumes. Based on solutions used in pulse stretching experiments, we introduce a double-pass scheme that reduces the errors produced through spatio-temporal coupling by at least one order of magnitude. Finally, employing single molecules as nanoscale probes, we prove that such a double pass scheme is capable of artifact-free pulse shaping at dimensions two orders of magnitude smaller than the diffraction limit.

OCIS codes: (020.1670) Coherent optical effects; (120.4820) Optical systems; (320.2250) Femtosecond phenomena; (320.5540) Pulse shaping; (320.7100) Ultrafast measurements; (320.7160) Ultrafast technology.

References and links

1. Y. Silberberg and D. Meshulach, "Coherent quantum control of two-photon transitions by a femtosecond laser pulse," Nature **396**(6708), 239–242 (1998).
2. J. L. Herek, W. Wohlleben, R. J. Cogdell, D. Zeidler, and M. Motzkus, "Quantum control of energy flow in light harvesting," Nature **417**(6888), 533–535 (2002).
3. V. I. Prokhorenko, A. M. Nagy, S. A. Waschuk, L. S. Brown, R. R. Birge, and R. J. D. Miller, "Coherent control of retinal isomerization in bacteriorhodopsin," Science **313**(5791), 1257–1261 (2006).
4. D. V. Voronine, D. Abramavicius, and S. Mukamel, "Coherent control protocol for separating energy-transfer pathways in photosynthetic complexes by chiral multidimensional signals," J. Phys. Chem. A **115**(18), 4624–4629 (2011).
5. A. Assion, T. Baumert, M. Bergt, T. Brixner, B. Kiefer, V. Seyfried, M. Strehle, and G. Gerber, "Control of chemical reactions by feedback-optimized phase-shaped femtosecond laser pulses," Science **282**(5390), 919–922 (1998).
6. T. Brixner and G. Gerber, "Quantum control of gas-phase and liquid-phase femtochemistry," ChemPhysChem **4**(5), 418–438 (2003).
7. V. V. Lozovoy and M. Dantus, "Systematic control of nonlinear optical processes using optimally shaped femtosecond pulses," ChemPhysChem **6**(10), 1970–2000 (2005).
8. C. D. Stanciu, F. Hansteen, A. V. Kimel, A. Kirilyuk, A. Tsukamoto, A. Itoh, and T. Rasing, "All-optical magnetic recording with circularly polarized light," Phys. Rev. Lett. **99**(4), 047601 (2007).
9. D. Hillerkuss, R. Schmogrow, T. Schellinger, M. Jordan, M. Winter, G. Huber, T. Vallaitis, R. Bonk, P. Kleinow, F. Frey, M. Roeger, S. Koenig, A. Ludwig, A. Marculescu, J. Li, M. Hoh, M. Dreschmann, J. Meyer, S. Ben Ezra, N. Narkiss, B. Nebendahl, F. Parmigiani, P. Petropoulos, B. Resan, A. Oehler, K. Weingarten, T. Ellermeyer, J. Lutz, M. Moeller, M. Huebner, J. Becker, C. Koos, W. Freude, and J. Leuthold, "26 Tbit s−1 line-rate super-channel transmission utilizing all-optical fast Fourier transform processing," Nat. Photonics **5**(6), 364–371 (2011).
10. Z. Jiang, C.-B. Huang, D. E. Leaird, and A. M. Weiner, "Optical arbitrary waveform processing of more than 100 spectral comb lines," Nat. Photonics **1**(8), 463–467 (2007).

#156834 - $15.00 USD Received 21 Oct 2011; revised 28 Nov 2011; accepted 28 Nov 2011; published 13 Dec 2011

11. P. Král, I. Thanopulos, and M. Shapiro, "Coherently controlled adiabatic passage," Rev. Mod. Phys. **79**(1), 53–77 (2007).
12. A. Greentree, S. Devitt, and L. Hollenberg, "Quantum-information transport to multiple receivers," Phys. Rev. A **73**(3), 032319 (2006).
13. H. Rabitz, R. de Vivie-Riedle, M. Motzkus, and K. Kompa, "Whither the future of controlling quantum phenomena?" Science **288**(5467), 824–828 (2000).
14. D. G. Kuroda, C. P. Singh, Z. Peng, and V. D. Kleiman, "Mapping excited-state dynamics by coherent control of a dendrimer's photoemission efficiency," Science **326**(5950), 263–267 (2009).
15. G. S. Engel, T. R. Calhoun, E. L. Read, T.-K. Ahn, T. Mancal, Y.-C. Cheng, R. E. Blankenship, and G. R. Fleming, "Evidence for wavelike energy transfer through quantum coherence in photosynthetic systems," Nature **446**(7137), 782–786 (2007).
16. E. Collini, C. Y. Wong, K. E. Wilk, P. M. G. Curmi, P. Brumer, and G. D. Scholes, "Coherently wired light-harvesting in photosynthetic marine algae at ambient temperature," Nature **463**(7281), 644–647 (2010).
17. D. Brinks, F. D. Stefani, F. Kulzer, R. Hildner, T. H. Taminiau, Y. Avlasevich, K. Müllen, and N. F. van Hulst, "Visualizing and controlling vibrational wave packets of single molecules," Nature **465**(7300), 905–908 (2010).
18. R. Hildner, D. Brinks, and N. F. van Hulst, "Femtosecond coherence and quantum control of single molecules at room temperature," Nat. Phys. **7**(2), 172–177 (2011).
19. W. Min, S. Lu, S. Chong, R. Roy, G. R. Holtom, and X. S. Xie, "Imaging chromophores with undetectable fluorescence by stimulated emission microscopy," Nature **461**(7267), 1105–1109 (2009).
20. B. G. Saar, C. W. Freudiger, J. Reichman, C. M. Stanley, G. R. Holtom, and X. S. Xie, "Video-rate molecular imaging in vivo with stimulated Raman scattering," Science **330**(6009), 1368–1370 (2010).
21. C. W. Freudiger, W. Min, G. R. Holtom, B. Xu, M. Dantus, and X. Sunney Xie, "Highly specific label-free molecular imaging with spectrally tailored excitation-stimulated Raman scattering (STE-SRS) microscopy," Nat. Photonics **5**(2), 103–109 (2011).
22. D. Zeidler, T. Hornung, D. Proch, and M. Motzkus, "Adaptive compression of tunable pulses from a non-collinear-type OPA to below 16 fs by feedback-controlled pulse shaping," Appl. Phys. B **131**, 125–131 (2000).
23. H.-S. Tan, E. Schreiber, and W. S. Warren, "High-resolution indirect pulse shaping by parametric transfer," Opt. Lett. **27**(6), 439–441 (2002).
24. D. Lorenc, D. Velic, A. Markevitch, and R. Levis, "Adaptive femtosecond pulse shaping to control supercontinuum generation in a microstructure fiber," Opt. Commun. **276**(2), 288–292 (2007).
25. T. Ganz, V. Pervak, A. Apolonski, and P. Baum, "16 fs, 350 nJ pulses at 5 MHz repetition rate delivered by chirped pulse compression in fibers," Opt. Lett. **36**(7), 1107–1109 (2011).
26. O. E. Martinez, J. P. Gordon, and R. L. Fork, "Negative group-velocity dispersion using refraction," J. Opt. Soc. Am. A **1**(10), 1003–1006 (1984).
27. E. Treacy, "Optical pulse compression with diffraction gratings," IEEE J. Quantum Electron. **5**(9), 454–458 (1969).
28. O. Martinez, "Design of high-power ultrashort pulse amplifiers by expansion and recompression," IEEE J. Quantum Electron. **23**(8), 1385–1387 (1987).
29. R. Szipocs, K. Ferencz, C. Spielmann, and F. Krausz, "Chirped multilayer coatings for broadband dispersion control in femtosecond lasers," Opt. Lett. **19**(3), 201–203 (1994).
30. T. Brixner and G. Gerber, "Femtosecond polarization pulse shaping," Opt. Lett. **26**(8), 557–559 (2001).
31. M. Aeschlimann, M. Bauer, D. Bayer, T. Brixner, F. J. García de Abajo, W. Pfeiffer, M. Rohmer, C. Spindler, and F. Steeb, "Adaptive subwavelength control of nano-optical fields," Nature **446**(7133), 301–304 (2007).
32. A. M. Weiner, "Femtosecond pulse shaping using spatial light modulators," Rev. Sci. Instrum. **71**(5), 1929–1960 (2000).
33. A. M. Weiner, D. E. Leaird, G. P. Wiederrecht, and K. A. Nelson, "Femtosecond pulse sequences used for optical manipulation of molecular motion," Science **247**(4948), 1317–1319 (1990).
34. A. M. Weiner, D. E. Leaird, J. S. Patel, and J. R. Wullert, "Programmable shaping of femtosecond optical pulses by use of 128-element liquid crystal phase modulator," IEEE J. Quantum Electron. **28**(4), 908–920 (1992).
35. A. M. Weiner, D. E. Leaird, J. S. Patel, and J. R. Wullert, "Programmable femtosecond pulse shaping by use of a multielement liquid-crystal phase modulator," Opt. Lett. **15**(6), 326–328 (1990).
36. P. Tian, D. Keusters, Y. Suzaki, and W. S. Warren, "Femtosecond phase-coherent two-dimensional spectroscopy," Science **300**(5625), 1553–1555 (2003).
37. N. Krebs, R. A. Probst, and E. Riedle, "Sub-20 fs pulses shaped directly in the UV by an acousto-optic programmable dispersive filter," Opt. Express **18**(6), 6164–6171 (2010).
38. R. Dixon, "Acoustic diffraction of light in anisotropic media," IEEE J. Quantum Electron. **3**(2), 85–93 (1967).
39. P. Tournois, "Acousto-optic programmable dispersive filter for adaptive compensation of group delay time dispersion in laser systems," Opt. Commun. **140**(4-6), 245–249 (1997).
40. F. Verluise, V. Laude, Z. Cheng, C. Spielmann, and P. Tournois, "Amplitude and phase control of ultrashort pulses by use of an acousto-optic programmable dispersive filter: pulse compression and shaping," Opt. Lett. **25**(8), 575–577 (2000).
41. F. Verluise, V. Laude, J. P. Huignard, P. Tournois, and A. Migus, "Arbitrary dispersion control of ultrashort optical pulses with acoustic waves," J. Opt. Soc. Am. B **17**(1), 138–145 (2000).
42. C. Dorrer and F. Salin, "Phase amplitude coupling in spectral phase modulation," IEEE J. Sel. Top. Quantum Electron. **4**(2), 342–345 (1998).

#156834 - $15.00 USD Received 21 Oct 2011; revised 28 Nov 2011; accepted 28 Nov 2011; published 13 Dec 2011

43. T. Tanabe, H. Tanabe, Y. Teramura, and F. Kannari, "Spatiotemporal measurements based on spatial spectral interferometry for ultrashort optical pulses shaped by a Fourier pulse shaper," J. Opt. Soc. Am. B **19**(11), 2795–2802 (2002).
44. A. Monmayrant, S. Weber, and B. Chatel, "A newcomer's guide to ultrashort pulse shaping and characterization," J. Phys. At. Mol. Opt. Phys. **43**(10), 103001 (2010).
45. D. J. McCabe, D. R. Austin, A. Tajalli, S. Weber, I. A. Walmsley, and B. Chatel, "Space–time coupling of shaped ultrafast ultraviolet pulses from an acousto-optic programmable dispersive filter," J. Opt. Soc. Am. B **28**(1), 58–64 (2011).
46. O. E. Martinez, "Grating and prism compressors in the case of finite beam size," J. Opt. Soc. Am. B **3**(7), 929–934 (1986).
47. N. H. Bonadeo, J. Erland, D. Gammon, D. Park, D. S. Katzer, and D. G. Steel, "Coherent optical control of the quantum state of a single quantum Dot," Science **282**(5393), 1473–1476 (1998).
48. D. Brinks, F. D. Stefani, and N. F. van Hulst, "Nanoscale spatial effects of pulse shaping," Springer Ser. Chem. Phys. **92**, 890–892 (2009).
49. B. Sussman, R. Lausten, and A. Stolow, "Focusing of light following a 4-f pulse shaper: considerations for quantum control," Phys. Rev. A **77**(4), 043416 (2008).
50. F. Frei, R. Bloch, and T. Feurer, "Influence of finite spatial resolution on single- and double-pass femtosecond pulse shapers," Opt. Lett. **35**(23), 4072–4074 (2010).
51. J. W. Goodman, *Introduction to Fourier Optics*, 3rd ed. (Roberts & Company Publishers, 2005).
52. M. Wefers and K. Nelson, "Space-time profiles of shaped ultrafast optical waveforms," IEEE J. Quantum Electron. **32**(1), 161–172 (1996).
53. A. Anderson, K. S. Deryckx, X. G. Xu, G. Steinmeyer, and M. B. Raschke, "Few-femtosecond plasmon dephasing of a single metallic nanostructure from optical response function reconstruction by interferometric frequency resolved optical gating," Nano Lett. **10**(7), 2519–2524 (2010).
54. D. Sadiq, J. Shirdel, J. S. Lee, E. Selishcheva, N. Park, and C. Lienau, "Adiabatic nanofocusing scattering-type optical nanoscopy of individual gold nanoparticles," Nano Lett. **11**(4), 1609–1613 (2011).
55. R. Hildner, D. Brinks, F. D. Stefani, and N. F. van Hulst, "Electronic coherences and vibrational wave-packets in single molecules studied with femtosecond phase-controlled spectroscopy," Phys. Chem. Chem. Phys. **13**(5), 1888–1894 (2011).
56. D. Strickland and G. Mourou, "Compression of amplified chirped optical pulses," Opt. Commun. **56**(3), 219–221 (1985).
57. M. M. Wefers and K. A. Nelson, "Analysis of programmable ultrashort waveform generation using liquid-crystal spatial light modulators," J. Opt. Soc. Am. B **12**(7), 1343–1362 (1995).
58. Y. Avlasevich, S. Müller, P. Erk, and K. Müllen, "Novel core-expanded rylenebis(dicarboximide) dyes bearing pentacene units: facile synthesis and photophysical properties," Chemistry **13**(23), 6555–6561 (2007).

1. Introduction

Many experiments in physics [1–4], chemistry [5–7], communication technology [8–10], and quantum information technology [11, 12] make use of shaped ultrafast laser pulses, e.g. for addressing dynamic processes in molecules [13–18], to optimize contrast in stimulated emission [19] or Raman spectroscopy [20, 21] and to enhance stability and output power in pulse amplification [22], parametric conversion [23], and supercontinuum generation [24, 25]. Compensation of acquired second and third order dispersion can be accomplished with pulse stretchers and compressors based on prisms [26], gratings [27, 28] or chirped mirrors [29], but for higher order or non-polynomial phase compensation these do not suffice. Moreover, experiments with few-femtosecond pulses often require sculpting the spectral amplitude [2, 3] or polarization [30, 31]. For these more intricate pulse-shaping actions, more advanced shapers that can address individual bands in the spectrum with high resolution are necessary.

The two most used pulse shaping techniques are based on Liquid-Crystal (LC) Spatial Light Modulators (SLMs) integrated in a 4f-configuration [32–35] and on Acousto-Optic Programmable Dispersive Filters (AOPDFs) [36–41].

In Fig. 1a a sketch of a 4f-shaper based on a LC SLM is shown. The frequency components of a laser pulse are dispersed spatially by a diffraction grating and then focused on an LC-array that is placed in the Fourier plane. Each pixel in the LC-array is a birefringent element, the optical length of which can be adjusted by applying a voltage, thus creating a spectrally dependent phase function. Simultaneous application of an extra mask can create a spectrally dependent polarization, since the change in optical length is accompanied by a gradual variation of the polarization state of the light passing through the pixel. After the LC the light is recollimated and the frequency components are recombined on a second grating to

#156834 - $15.00 USD Received 21 Oct 2011; revised 28 Nov 2011; accepted 28 Nov 2011; published 13 Dec 2011

form the output pulse. A polarizer after the shaper projects the spectral polarization function into an amplitude modulation if desired.

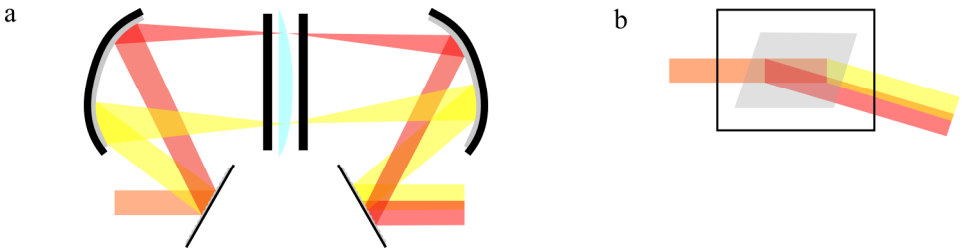

Fig. 1. The standard single-pass configurations of pulse shapers based on a) Spatial Light Modulators (SLM) and b) Acousto-Optic Programmable Dispersive Filters (AOPDF). In both cases, different phase shifts applied to different spectral components will cause a spatial displacement in the output beam; this is called spatio-temporal coupling.

In AOPDFs (Fig. 1b) laser pulses are shaped by interaction with an acoustic pulse in a birefringent crystal [38]. The phase matching requirement for efficient acousto-optic interaction leads to control of the position in the crystal where the optical and acoustic pulses interact, through dispersion of the acoustic spectrum. The amplitude and phase modulations of the acoustic spectrum are in this way imprinted on the optical spectrum [39, 40].

Pulse shaping is generally performed in a single-pass configuration [1–3,5–10,13,14,19–25, 30–40] (Figs. 1a and b). In this context, we define 'single pass' as one complete passage of a pulse through a shaper, that is, in AOPDF-based shapers one pass through the crystal, and in SLM-based 4f-shapers one sequence of dispersion, focusing, shaping, collimation, and frequency recombination.

This article discusses the nature and magnitude of spatio-temporal coupling induced by single-pass shaping [42–44], shows its adverse effect on typical coherent control experiments and presents solutions, most importantly in the form of a double pass through a pulse shaper. As an example of coupling-free pulse shaping the excitation of vibrational wavepackets in a single molecule is presented.

2. Experimental

The spatio-temporal coupling induced in shaped laser pulses was studied in detail using nanoparticles and single molecules as local field probes. Shaped and pre-compensated pulses were directed into a confocal microscope and focused with a 1.3 NA objective (Fluar, Zeiss) onto a thin microscope cover slip containing a sample layer with a few nanometer thickness. The full-width at half maximum of the focus ranged from 250 to 300 nm depending on the experiment. The signal recorded from the sample was always the single photon excited fluorescence, which was separated from the excitation light using suitable dichroic beam splitters and long pass filters, and detected by an avalanche photodiode (APDs, Perkin Elmer, SPCM-AQR-14). The excitation power was simultaneously recorded with a photodiode at the sample position and was typically in the range of a few µW. The sample position is controlled with a precision of about 1 nm using a closed-loop piezo stage (Mad City Labs). A measurement started with scanning the sample to image the fluorescence intensity as a function of position. This allows for localization of nanoparticles or single molecules in the sample, which are consecutively brought into the focus of the excitation beam. The fluorescence signal is then recorded as function of the position and the applied pulse shape.

In a first experiment, the pulses were produced by an optical parametric oscillator (OPO, Automatic PP, APE, pumped by a Titanium:Sapphire-system, Mira, Coherent). The resulting pulse train was passed through a pulse picker (PulseSelect, APE) to reduce the repetition rate from 76 MHz to effectively 1.25 MHz (bunches of pulses with a repetition rate of 25 kHz, repetition rate within bunches: 10 MHz). The pulses in this experiment were shaped with an

#156834 - $15.00 USD Received 21 Oct 2011; revised 28 Nov 2011; accepted 28 Nov 2011; published 13 Dec 2011

acousto-optic programmable dispersive filter (AOPDF, Dazzler, Fastlite). This shaper was used for dispersion compensation, to provide transform limited pulses with 50 fs duration at the sample plane, as well as for shaping to generate pulse sequences with a well defined delay time Δt and relative phase. This shaped beam was inspected by direct imaging onto a CCD camera (Andor).

In a second experiment, the pulses were provided in an 85 MHz pulse train by a broadband Titanium Sapphire laser (Octavius 85 M, Menlo Systems) that was tuned to a center wavelength of 676 nm. The resulting pulses had a spectral bandwidth of 120 nm and were compressed to 14 fs in the sample plane. For dispersion compensation and shaping a 4f-shaper based on a double-pass spatial light modulator was used (adapted from MIIPS-box, Biophotonics Solutions Inc).

3. Results and Discussion

3.1 Experimental quantification of spatio-temporal coupling

Adding spectral phase to a pulse in a single pass shaper spatially disperses the frequency components of the output pulse as sketched in Fig. 1.

A 4f-shaper theoretically forms an ideal telescope with a magnification of one. The spot of the incoming beam on the first grating can be viewed as an object that will be imaged perfectly on the second grating. An SLM with a phase function applied can be viewed as a discretized cylindrical Fresnel lens; when placed in the fourier plane of the shaper it will modify the imaging properties of the telescope. As a result, the "image" will be magnified along the shaping direction on the second grating. Since the light is diffracted by the first grating, with an angle proportional to the wavelength, the magnified image will additionally exhibit a spatial dispersion of wavelengths equal to the "magnification" introduced by the lensing action of the phase mask applied on the SLM.

In an AOPDF, the laser pulse propagates through a chirped Bragg grating, created by the applied acoustic pulse, which refracts different wavelengths at different positions in the crystal. Because of the phase matching condition, the acoustic wave is launched with a k-vector non-collinear to that of the laser beam; the outgoing laser beam therefore has a modified propagation direction according to $k_{out}=k_{in}+k_{acc}$ [41]. This change of direction at different points in the crystal for different wavelengths causes a spatial chirp accompanied by a broadening of the beam profile [45].

The spatio-temporal coupling created by these shaping processes has two main negative consequences. First, the non-ideal recombination of frequencies after the shaping action puts a limit on the spectral bandwidth available at each spatial coordinate in the laser beam [46]. It is therefore impossible to compress a pulse to the theoretical Fourier limit, which reduces-temporal resolution and peak power available in experiments. Second, simultaneous application of a spectral amplitude modulation and a phase modulation will cause an additional spatial modulation of the intensity across the beam profile [37]. This is illustrated with the beam images shown in Fig. 2, corresponding to a pulse with a 30 nm spectral bandwidth shaped in an AOPDF. The shaping action consists of a -36000 fs^2 phase mask for dispersion compensation and an additional cosinusoidal (Fig. 2a) or sinusoidal (Fig. 2b) amplitude modulation to create two pulses with 100 fs delay and 0 or π mutual phase difference, respectively. The difference between the two profiles (Fig. 2c) clearly reveals regular spatial intensity variations across the beam of up to 30%, caused by the spectral amplitude modulation.

#156834 - $15.00 USD Received 21 Oct 2011; revised 28 Nov 2011; accepted 28 Nov 2011; published 13 Dec 2011

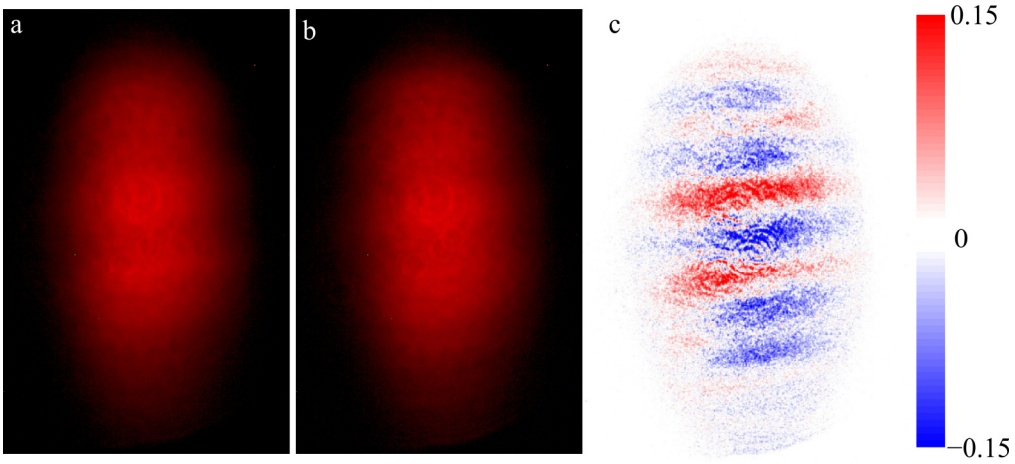

Fig. 2. a-b: Spatial profiles of a laser beam with 20 nm spectral bandwidth after passing through a single-pass AOPDF-based shaper. A cosinusoidal (a) and sinusoidal (b) amplitude modulation is applied on top of a –36000 fs^2 compensation phase to create two phase-locked pulses with 0 and π phase difference, respectively, and 100 fs delay time. c: The difference between the images in a and b reveals clear spatial intensity modulations of up to 30% of the local intensity.

A spectrally and therefore spatially modulated beam will be focused differently according to the Fourier principle. Coherent control experiments are generally influenced by this effect, because of their dependence on the overlap of three volumes: The excitation volume, the sample volume, and the detection volume. The excitation volume is defined by the focal volume of a shaped pump beam. The detection volume is given by the focal volume of a probe beam or the projection of a detector-area into the sample. The sample volume is the space occupied by the system under investigation.

In bulk experiments in liquids or solids, where the sample is uniform, the sample volume is irrelevant as long as it is larger than the excitation and detection volumes in every dimension. However, in experiments on non-uniform samples the effective sample volume becomes important, as it is determined by the spatial distribution of the sample unit under investigation (e.g. molecular beams, single molecules [18, 19], nanoparticles [31], quantum dots [47]). A changing position of the excitation volume as a function of temporal pulse shape, will cause a varying overlap with finite sized detection and sample volumes and result in a varying signal irrespective of any temporal dynamics in the sample.

An example of effects produced by spatio-temporal coupling and limited sample, excitation and detection volumes is shown in Fig. 3, which presents the results of a degenerate pump-probe experiment on gold nanoparticles (see experimental section). The roughly spherical particles with a diameter of 100 nm define the sample volume; the pump focus is nominally ~250 nm FWHM along the smallest dimension but is elongated due to the elliptical profile of the shaped excitation beam. The imaged detector area is about 2 μm, and the centers of the pump and detection volumes overlap. The sample is scanned through those volumes to obtain an image as shown in Fig. 3a. (Convolution of the particle size with the excitation volume determines the spot sizes in the image.) A nano-particle is then placed at different positions in the pump focus and excited with two phase-locked pulses generated by the AOPDF (see above) with a sinusoidal amplitude modulation of the pulse spectrum applied on top of a phase modulation to compensate for 36000 fs^2 dispersion of the setup. The inter-pulse delay is varied from 0 to 300 fs and the phase between the pulses is locked at 0 rad.

We chose 100 nm gold particles for this experiment because they are comparable in size to the focus and therefore show that artifacts do not only play a role on scales very much smaller than the focal volume (i.e. the excitation volume). In addition, since the signals are linear with

#156834 - $15.00 USD Received 21 Oct 2011; revised 28 Nov 2011; accepted 28 Nov 2011; published 13 Dec 2011

excitation power and the absorption spectrum of the gold particles is much broader than the pulse bandwidth, no signal change as a function of temporal pulse shape is expected. However, as shown in Fig. 3b, the signal of the nanoparticles presents strong variations as a function of the applied pulse shape. Moreover, the result of the experiment varies dramatically depending on the position of the gold particle in the focus, with the largest difference occurring between the particle in the top and bottom side of the focus (red and magenta curves).

This is a consequence of two effects: i) a variation of the beam width, and ii) changes in the symmetry of the beam profile. At short delays the application of the spectral amplitude-mask has, through spatio-temporal coupling, the effect of a "breathing" of the beam width, with the beam first getting narrower and then wider with increasing delays. This means the excitation focus will get wider and subsequently narrower with delay [48]. Depending on the position of the particle, this causes a better or worse overlap of the excitation volume with the gold particle, which results in higher or lower signals for particular delays depending on the particle position, as Fig. 3 shows. In addition the exact shape of the spectrum is important, as an asymmetric spectrum will cause an asymmetric beam profile after single pass shaping, which will thus be focused lopsided. Introducing a spectral amplitude modulation will therefore cause translational motions of the excitation volume on top of the breathing of the focal size.

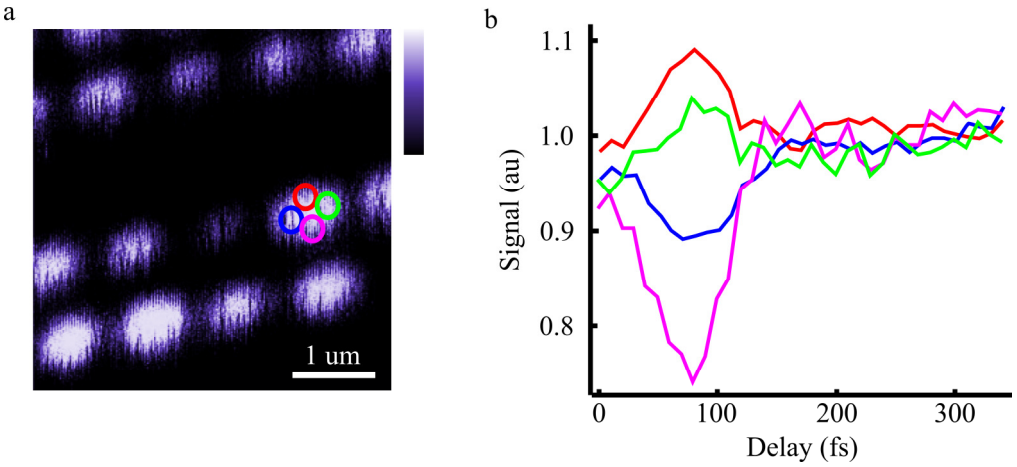

Fig. 3. a) 5x5 μm^2 scan of a sample of regularly arranged gold-nanoparticles with a diameter of 100 nm. The emission intensity is color coded with high signal indicated by white. b) Normalized photoluminescence as a function of inter-pulse delay at constant phase difference for a single Au-particle placed at different positions in the excitation focus, indicated by the colored circles in a. Here, the pulse sequences were created with a single-pass AOPDF.

This variation of position and size of the excitation volume with the pulse shape, as illustrated in Fig. 3, can have profound influence on coherent control experiments. The changing overlap between excitation, sample and detection volume leads to artificial signal fluctuations as a function of applied pulse shape, which can steer the outcome of optimization routines in coherent control experiments towards undesired target states. Moreover, after an optimization routine influenced by this artifact, an examination of pulses perceived as optimized to achieving a particular target state will lead to incorrect deductions about the molecular energy landscapes involved.

Spatio-temporal coupling is the natural result of optical transformations fundamentally limited by diffraction. Spatial shifts of finite-sized beams cause the coupling between space and time in AOPDFs; diffraction of finite-sized beams is its source in 4f-shapers; diffraction limited propagation and focusing cause a finite excitation volume, preventing ideal spatial and temporal recombination of the resulting pulse in a sample.

#156834 - $15.00 USD Received 21 Oct 2011; revised 28 Nov 2011; accepted 28 Nov 2011; published 13 Dec 2011

The spatial effects of spatio-temporal coupling influence each type of pulse shaping experiment differently: in principle, they could cancel out when both sample and detection volume are uniform and larger than any spatial change in the excitation beam, for example when using detectors with a projected area significantly larger than the pump focus in a uniform sample. This cancelling however, is not possible in the case of experiments utilizing probe beams for signal read-out, due to the non-uniform spatial nature of beam foci, and therefore of the detection volume. Experiments on structured samples, e.g. single molecules, nanostructures, quantum dots, and biological structures such as membranes or cells, by their very nature do not have a uniform sample volume and will therefore be influenced by this effect independent of the detection method.

Furthermore, this relaxing of the experimental conditions does not hold for experiments involving nonlinear process, because the excitation power density does vary locally, which will change the overall outcome of multiphoton process even when integrated spatially. Finally, the temporal effect of spatio-temporal coupling, i.e. the limit imposed on time resolution by non-ideal frequency recombination and the smaller effective bandwidth utilized, cannot be overcome this way. To achieve this, the spatio-temporal coupling needs to be canceled in the shaping process itself.

3.2 Fourier analysis of spatio-temporal coupling in 4f – pulse shapers

To gain a more detailed understanding of the way a shaper induces spatio-temporal coupling we performed a Fourier analysis of the passage of a pulse through a single-pass 4f-shaper.

We note that space-time coupling in shapers is often treated in terms of pixilation effects in SLMs [49, 50]. This paper aims to show that even in an ideal, non-pixilated shaper spatio-temporal coupling is a source of artifacts. As the effect of full and limited pixilation in LC-arrays has been investigated elsewhere [49, 50], we focus here on the purely geometrical effects induced in a 4f-shaper. We therefore represent the pulse spectrum as well as the phase and amplitude modulations as continuous in frequency space.

The laser pulse is modeled with a Gaussian spatial cross-section and a Gaussian spectral profile in the x-z-plane propagating along the z-direction. The dispersion on the grating as well as the shaping action is along the x-coordinate. As the action of the focusing elements is equal along x and y, and the beam is propagated as a Gaussian in both x and y, the laser pulse is described as a 2-dimensional Gaussian in x-ω or x-λ space. The beam undergoes the following transformations [49, 51, 52]:

1. Dispersion on the first grating according to

$$E_1(x,\omega) = \sqrt{\beta} E_{in}(\beta x,\omega)\exp[i\gamma(\omega-\omega_0)x] \tag{1}$$

with $\beta = \cos\theta_i / \cos\theta_d$, $\theta_{i(d)}$ being the angle of incidence (diffraction) of the central frequency ω_0 on the grating; and $\gamma = 2\pi\,(d\omega_0\cos\theta_d)^{-1}$, with d being the line spacing of the grating.

2. Propagation from the grating to the first focusing element according to

$$E_2(k,\omega) = E_1(k,\omega)\exp[\frac{-ik^2 f\lambda_0}{4\pi}] \tag{2}$$

where $E_1(k,\omega)$ represents the spatial Fourier transform of $E_1(x,\omega)$, f denotes the focal length of the focusing elements, which is the propagation distance from the grating to the first focusing element, and $k = 2\pi/x$;

3. Focusing of the beam according to

$$E_3(x,\omega) = E_2(x,\omega)\exp[\frac{-i\pi x^2}{f\lambda_0}] \tag{3}$$

#156834 - $15.00 USD Received 21 Oct 2011; revised 28 Nov 2011; accepted 28 Nov 2011; published 13 Dec 2011

4. Propagation from the focusing element to the shaping plane over a distance of *f* according to (2);

5. Shaping action according to

$$E_5(x,\omega) = E_4(x,\omega)T_{mask}(x) \tag{4}$$

with $T_{mask}(x)$ being a complex function $A(x)e^{i\phi(x)}$ for amplitude and phase shaping;

6. Propagation from the shaping plane to the second focusing element according to (2)

7. Collimation according to (3);

8. Propagation from the focusing element to the second grating according to (2);

9. Recombination according to

$$E_9(x,\omega) = \sqrt{1/\beta}E_8(x/\beta,\omega)\exp[i\gamma(\omega-\omega_0)x/\beta] \tag{5}$$

10. Propagation out of the shaper according to (2).

The output field after a single-pass shaper can thus be written as

$$E_{out}(k,\omega) = E_{in}(k,\omega)T_{single}(k,\omega) \tag{6}$$

with

$$T_{single}(k,\omega) = T_{mask}(-\frac{\gamma(\omega-\omega_0)-\beta k}{2\pi}\lambda_0 f) \tag{7}$$

Here $T_{mask}(x)$ is the spatial shaping function as defined in (5). The (k,ω)-content of each *x*-coordinate is determined by β and γ; βk gives the spatial dispersion induced by the part of the *k*-space occupied by the beam; $\gamma(\omega-\omega_0)$ represents the dispersion induced by the grating.

In the shaping plane a negative quadratic dispersion is added to the pulse to pre-compensate dispersion by optical elements. Since quadratic dispersion through spatial phase application effectively creates a lens, T_{mask} can be expressed as $T_{mask} = \exp[\frac{-i\omega_0 x^2}{2cl_m}]$, where l_m is the equivalent focal length of the applied quadratic phase mask.

As the coordinate transformation $x \to -\frac{\gamma(\omega-\omega_0)-\beta k}{2\pi}\lambda_0 f$ yields a T_{single} with a cross term between *k* and ω, it follows that there is a coupling between the dominant wavelength and the x-coordinate in the beam.

This analysis is illustrated in the top row of Fig. 4, which shows the simulation of a single-pass shaper for an initial Gaussian spectral and spatial profile of the beam in x- and λ-dimension (Fig. 4a) with a beam diameter of 2 mm (FWHM) and a spectral bandwidth of 20 nm ($6*10^{13}$ rad/s) centered at λ_0 = 800 nm. In this example an amplitude modulation is applied to create phase-locked pulses with 50 fs delay and 0 phase shift (Fig. 4b) and 50 fs delay and π phase difference (Fig. 4c), and simultaneously, −25000 fs^2 dispersion is added to this amplitude mask. The value of −25000 fs^2 is in the range of what is typically needed to compensate for passage through several optical elements and an objective. Although the pulses have the desired spectral characteristics if integrated over the entire spatial profile (Fig. 4b,c, red and blue curves), the 2D plots demonstrate that their spectral content varies significantly over the beam profile. Moreover, their spatial intensity profile differs from that of the unshaped beam (Fig. 4d). Both the broadening of the beam due to the spatio-temporal coupling as well as the spatial intensity modulation resulting from the applied spectral amplitude modulation is clearly visible (see also the experimental data in Fig. 2).

#156834 - $15.00 USD Received 21 Oct 2011; revised 28 Nov 2011; accepted 28 Nov 2011; published 13 Dec 2011

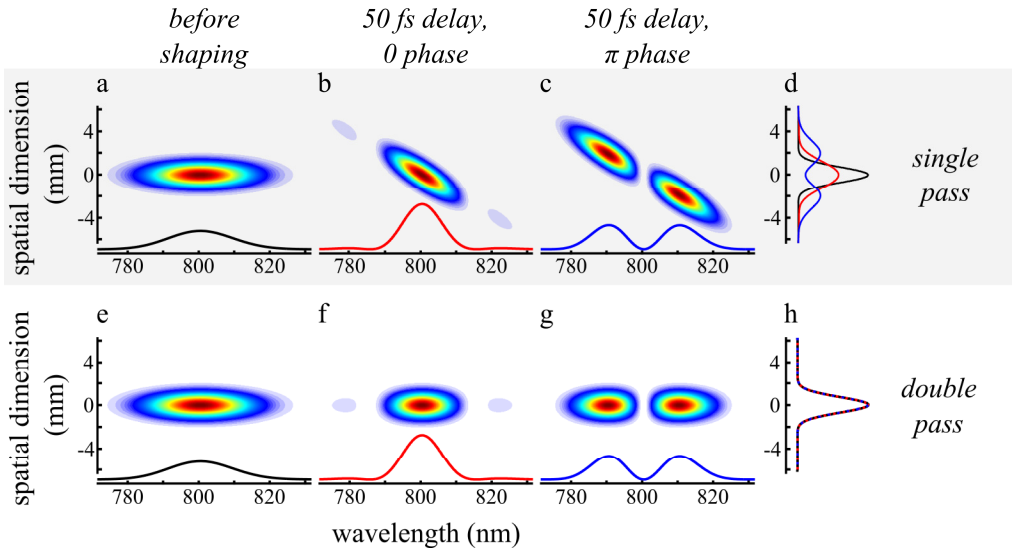

Fig. 4. A laser beam with Gaussian spatial and spectral profile is propagated through a single-pass (top row, a-d) and a double-pass 4f-pulse shaper (bottom row, e-h), respectively. For both shaper configurations a quadratic phase mask is applied to compensate for 25000 fs^2 dispersion and an additional amplitude mask is imprinted to create a phase-locked pulse pair with 50 fs delay and 0 (π) rad relative phase. The intensity profiles of the beam are shown in a wavelength-space (λ-x) frame (a-c and e-g), together with the integrated spectral intensity below each profile for the incoming (a,e, black curve), 0 phase (b,f, red curve), and π phase shaped beam (c,g, blue curve).The corresponding integrated spatial intensity profiles are depicted in the rightmost panel (d,h).

3.3 Reduction and compensation of spatio-temporal coupling

Diffraction being the limiting factor in obtaining correct pulse shapes suggests that relaxing the requirements for complete overlap of all spectral and spatial components of the beam can function as a patch solution to reduce the effects caused by spatio-temporal coupling. For certain classes of experiments this can be accomplished by scanning sample and detector area through the pump beam and averaging the signal over the entire pump area, effectively making them uniform in the excitation volume [17]. Another approach is manipulation the pulse beyond far field optical transformations, i.e. using near field optics [53, 54] or spatial filtering [17, 18, 55] to force a particular spatial mode on the pulse.

While in principle allowing for cleaned up coherent control experiments, these solutions are not ideal. Instead of canceling out the effects spatio-temporal coupling causes, this approach only reduces their magnitude, and therefore has to be adapted to and checked before each experiment. Whether the residual effects will be negligible compared to the actual signal depends on the experiment. Especially for coherent control experiments utilizing optimization routines based on genetic algorithms, it is virtually impossible to estimate beforehand whether the artifact level will have been reduced enough. It is equally hard to disentangle the artifact from an actual temporal effect in hindsight. Moreover, these solutions do not lift the limit spatio-temporal coupling imposes on the spectral bandwidth in the output pulse.

An ideal solution would result in a beam that: i) exhibits no spatio-temporal coupling after shaping independently of the specific shaping action, ii) utilizes the full bandwidth and all available power in the beam, and iii) is applicable in any experiment. Hence, the spatial part of the optical transformations that causes the spatio-temporal coupling should be reversed, without losing the temporal transformations on the pulse to be shaped.

High power, ultrafast laser and parametric amplification experiments suffered from a similar problem with pulse stretchers and compressors based on prisms and gratings. Passage through two prisms or gratings for stretching or compression purposes will result in

#156834 - $15.00 USD Received 21 Oct 2011; revised 28 Nov 2011; accepted 28 Nov 2011; published 13 Dec 2011

collimated beams at the output, but any temporal stretching or compression of the pulse will cause a spatial dispersion of frequencies in the output beam. Especially pulse stretchers are direct precursors of the common 4f-shaper. It was realized long ago that stretching pulses in a single pass configuration would not allow the pulse to be recompressed to the theoretical Fourier limit. An elegant solution was found by Martinez and others: placing a mirror at the end of the beam path and sending the pulses back through the stretcher. This arrangement gives the pulse double the stretching in the temporal domain and cancels out the spatial dispersion [28, 48, 56]. In the following we analyze this double-pass approach theoretically and describe its application to a 4f-shaper.

3.4 Fourier analysis of the effect of the 4f-double pass scheme on spatio-temporal coupling

In the simulation of a double-pass shaper the pulse undergoes transformations 1-10 followed by a mirror transformation, after which it goes through transformations 1-10 again. Applied to $E_{\mathrm{in}}(k,\omega)$, the transformation of the second pass is inverted in k-space compared to the transformation of the first pass due to the telescoping action of the first pass through the shaper. It can therefore readily be seen that the total output of a double pass shaping action is

$$E_{out}(k,\omega)=E_{in}(k,\omega)T_{double}(k,\omega) \tag{8}$$

with

$$T_{double}(k,\omega)=T_{mask}(-\frac{\gamma(\omega-\omega_0)-\beta k}{2\pi}\lambda_0 f)T_{mask}(-\frac{\gamma\left(\omega-\omega_0\right)+\beta k}{2\pi}\lambda_0 f) \tag{9}$$

In order to directly compare the single- and double-pass configurations, T_{mask} is adapted. In the latter scheme the pulse passes through the shaper twice, so the amplitude modulation is changed to its square root, and the applied phase is halved. The result after a forward and backward pass is a pulse with identical spectral amplitude modulations (Fig. 4f, g and insets) as compared with the single-pass configuration (Fig. 4b,c and insets). As can be seen from the 2D figures, however, the coupling between the spatial and spectral coordinates is absent and every point in the beam has the same spectral content. As a result, the output beam possesses the same Gaussian spatial profile as the input beam independent of the pulse shape (Fig. 4h).

Spatio-temporal coupling in pulse shapers has been analyzed before both experimentally and theoretically [32]. An influential theoretical comparison between the performance of the double-pass and single-pass shaper has been performed by Wefers and Nelson [52, 57], where the output of a double pass shaper is effectively defined by the same formula as (9). However, the sign inversion between $-\beta k$ and $+\beta k$ in the first and second pass was given as reason for not applying a double pass implementation as it implies an asymmetry between the forward and backward paths through the shaper and therefore a sustained spatio-temporal coupling. The double pass configuration is subsequently dismissed as apparently not reversing the spatio-temporal coupling, but instead creating a more complicated coupling between spectral and spatial content of the shaped beam.

In the context of our paper it is worth taking another look at this reasoning with an eye on modern equipment. Through the $x\rightarrow-\frac{\gamma(\omega-\omega_0)\pm\beta k}{2\pi}\lambda_0 f$ coordinate transformation the βk term propagates as an error on $\gamma(\omega-\omega_0)$ in the $T_{mask}(x)$ function. Any continuous mask function can be written as a summation of Fourier components, which in turn can be expanded in a summation over a collection of Taylor series. In the double-pass shaper, the error βk is perfectly canceled in first and second order terms of a Taylor expansion. This means that Eq. (7) becomes separable and the spatio-temporal coupling is completely reversed for first and second order polynomial masks. In higher order masks, the error propagates no larger than $O([\beta k]^2)$, which is in stark contrast to the shaping in single pass, where the error always propagates as $O(\beta k)$ or larger if a spectral phase is applied. The error caused by spatio-

#156834 - $15.00 USD Received 21 Oct 2011; revised 28 Nov 2011; accepted 28 Nov 2011; published 13 Dec 2011

temporal coupling in double pass shaping is therefore either cancelled completely or at least one order of magnitude smaller than in the equivalent shaping action in a single pass configuration.

We note that the resultant uncoupling does not mean that a spectral amplitude shape is not influenced by the spatio-temporal coupling inside the confines of the shaper. Especially for higher order masks a correction can be necessary to create the desired spectral amplitude shape. This is possible if the amplitude is obtained with a spectral polarization rotation mask and after passage through the double-pass shaper a linear polarization is projected out. Because polarization and phase are uncoupled transformations and the polarization transformation is unitary (as opposed to a hard amplitude transformation in the shaping plane, which will indeed produce more complicated and fundamentally uncorrectable shapes in a double pass configuration, as correctly pointed out by Wefers and Nelson), a polarization shape is influenced by the coupling between ω and k in the same order as a phase shape. It follows that it is generally possible to define a desired continuous polarization shape as a function of $\gamma(\omega-\omega_0)$ with error no larger than $O([\beta k]^2)$.

3.5 Experiment on single molecule dynamics free of spatio-temporal coupling

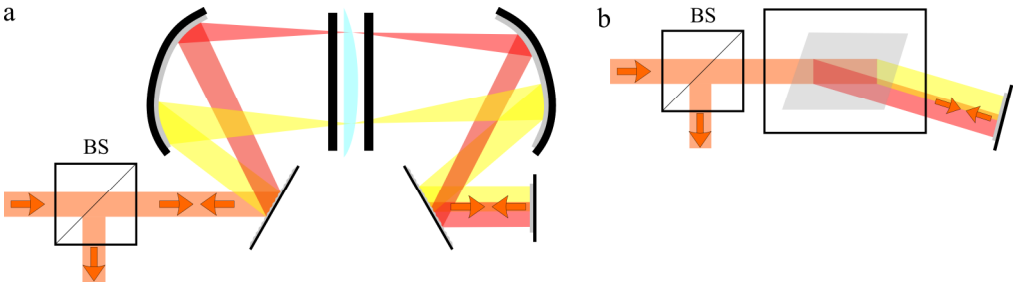

Fig. 5. Practical implementation of double-pass shapers based on (a) SLMs and (b) AOPDFs by passing the beam through a beam splitter (BS) and putting a mirror at the output of the shaper.

The implementation of the double pass schemes are sketched in Fig. 5 for both the 4f- and AOPDF-based shaper. In the 4f-shaper this can simply be realized by placing a 50-50 beam splitter (BS) at the entrance of the shaper and a mirror at the exit. This will, however, result in a power loss of a factor of four. In order to increase the output power, the 50-50 beam splitter can be replaced by a polarizing beam splitter. Recalibration of the amplitude transformations (A) in the LC-mask, according to $A_{new}(\omega) = 1\text{-}A_{old}(\omega)$, will provide the correct amplitude modulation at the output. Alternatively, it is possible to insert a $\lambda/4$ retardation plate at the output of the shaper, right before the mirror. Note that such schemes cannot be employed in shapers that are also meant to provide polarization shapes at the output. Another solution is to use the 3rd dimension, such that input and output beams are at different heights and no beam splitter at all is necessary.

Due to the small active area in AOPDFs and the dependence on the incoming polarization of the shaping action, such power optimization schemes cannot be employed. However, the basic double pass scheme with a 50-50 beam splitter and a mirror functions as well.

To test the performance of the double-pass scheme we performed measurements analogous to those on gold nanoparticles, but using single fluorescent molecules instead. Employing single molecules to probe spatial variations of the field has the important advantage that they provide a much higher spatial resolution. The fluorophores we used (the terrylene homologue DNQDI [58]) have a size, and thus provide a spatial resolution, of about 2 nm.

#156834 - $15.00 USD Received 21 Oct 2011; revised 28 Nov 2011; accepted 28 Nov 2011; published 13 Dec 2011

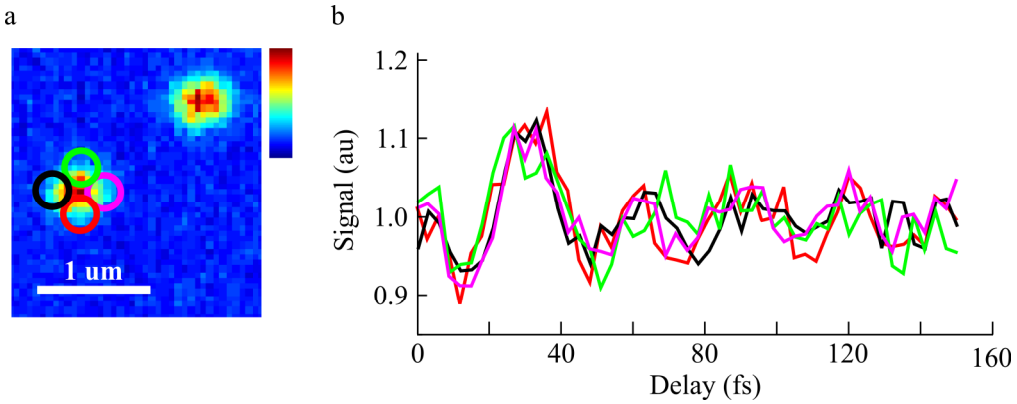

Fig. 6. a) Scan of a sample containing single DNQDI molecules with a size of about 2 nm. The emission intensity is color coded from blue to red. b) Normalized fluorescence as a function of delay and constant phase difference between the excitation pulse pair for a single DNQDI molecule placed at different positions in the excitation focus indicated by the colored circles in a.

In this experiment, we employed pulses from the Octavius, shaped with a double-pass 4f shaper (see above). Through amplitude shaping on top of the pulse compression, we created a phase-locked double pulse. We varied the delay between the two pulses between 0 and 150 fs and kept the relative phase locked at 0 rad. As can be seen in the example of Fig. 6, the signal from a single molecule oscillates as a function of the delay between the two pulses. In contrast to the measurements using single-pass pulse shapers, repeating the measurement at different positions in the focus shows no changes in the signal. The same oscillatory behavior is observed for all positions, demonstrating that the field presents no spatial variations whatsoever. Rather than an artifact product of spatial field variations, this oscillatory trace is a signature of temporal molecular dynamics due to vibrational wave-packet interference [17, 55]. The diffraction limited excitation spot in this experiment is ~300 nm (FWHM), whereas DNQDI has a size of ca. 2 nm. The insensitivity of this measurement to the position of a 2 nm sample in the 300 nm excitation spot shows that pulse shaping free of diffraction-based spatio-temporal artifacts was achieved with a resolution approximately 2 orders of magnitude beyond the diffraction limit. The importance of correcting for spatio-temporal coupling is demonstrated by the fact that the magnitude of the signal variations obtained with uncorrected beams is comparable to the real molecular signals obtained in these types of measurements; i.e. the vibrational wavepacket oscillations would almost totally be obscured by the spatio-temporal coupling artifact.

4. Conclusion

We have shown that pulse shapers in the general single-pass configuration introduce a spatio-temporal coupling in laser pulses that can severely influence ultrafast spectroscopy and coherent control measurements. The magnitude of the spatial effects caused by spatio-temporal coupling depends on the spectral modulations applied to the shaped pulse, on the steepness of the phase gradients created in the shaping mask, and on the relative sizes and spatial uniformity of the excitation, sample and detection volumes in the experiment. Through experiments on single gold nanoparticles we have demonstrated the significant magnitude of these effects. Theoretically, spatio-temporal coupling can be canceled out or significantly diminished with pulse shapers in a double-pass configuration. By using single fluorescent molecules as local probes of the electric field, we have demonstrated with a resolution of 2 nm that the double-pass pulse shaping produces homogeneous shaped fields. This kind of correction is essential to obtain reliable information in experiments using shaped laser pulses.

#156834 - $15.00 USD Received 21 Oct 2011; revised 28 Nov 2011; accepted 28 Nov 2011; published 13 Dec 2011

Acknowledgments

We thank Tim Taminiau and Florian Kulzer for discussions and assistance with the experimental setup, and Klaus Müllen for providing the molecules. We also appreciate technical assistance of Peter Fendel (Menlo Systems, IdestaQE) with the Octavius laser system, and the collaboration with Biophotonics Solutions Inc. in developing a dedicated pulse shaper. Funding by the Spanish ministry of science and innovation MICINN (CSD2007-046-NanoLight.es, MAT2006-08184 and FIS2009-08203), Fundació CELLEX Barcelona and the European Union (FP6 Bio-Light-Touch and ERC Advanced Grant 247330) is gratefully acknowledged.

#156834 - $15.00 USD Received 21 Oct 2011; revised 28 Nov 2011; accepted 28 Nov 2011; published 13 Dec 2011